Available online at www.sciencedirect.com

ScienceDirect

Procedia Manufacturing 38 (2019) 564–572

Procedia MANUFACTURING

www.elsevier.com/locate/procedia

29th International Conference on Flexible Automation and Intelligent Manufacturing (FAIM2019), June 24-28, 2019, Limerick, Ireland.

Flexible calibration of a stereo vision system by active display

Sandro Barone[a], Paolo Neri[a,*], Alessandro Paoli[a], Armando Viviano Razionale[a]

[a]*University of Pisa, Deparment of Civil and Industrial Engineering, Largo L. Lazzarino 1, Pisa 56122, Italy*

Abstract

Camera calibration plays a fundamental role for 3D computer vision since it is the first step to recover reliable metric information from 2D images. The calibration of a stereo-vision system is a two-step process: firstly, the calibration of the individual cameras must be carried out, then the two individual calibrations are combined to retrieve the relative placement between the two cameras, and to refine intrinsic and extrinsic parameters. The most commonly adopted calibration methodology uses multiple images of a physical checkerboard pattern. However, the process is time-consuming since the operator must move the calibration target into different positions, typically from 15 to 20. Moreover, the calibration of different optical setups requires the use of calibration boards, which differ for size and number of target points depending on the desired working volume. This paper proposes an innovative approach to the calibration, which is based on the use of a conventional computer screen to actively display the calibration checkerboard. The potential non-planarity of the screen is compensated by an iterative approach, which also estimate the actual screen shape during the calibration process. The use of an active display greatly enhances the flexibility of the stereo-camera calibration process since the same device can be used to calibrate different optical setups by simply varying number and size of the displayed squared patterns.

Keywords: Stereo camera calibration; Active display; Reverse Engineering; Structured light scanner.

* Corresponding author. Tel.: +39-050-2218010; fax: +39-050-2218069.
E-mail address: paolo.neri@dici.unipi.it

10.1016/j.promfg.2020.01.071

1. Introduction

The retrieval of reliable 3D surface information has become one of the most attractive research areas within optical metrology. 3D shape measurement techniques have penetrated a wide number of engineering areas: from industrial design [1], to flexible and intelligent manufacturing [2, 3], from cultural heritage [4], to virtual reality [5]. Many other applications may also benefit from 3D shape measurement technologies as manufacturing inspection [6], architecture [7], or bioengineering [8]. In this context, optical methods have considerably replaced contact methods (i.e., coordinate measurement machines) in all those applications which require high measurement efficiency in terms of time, cost and resolution [9]. Among these approaches, structured light (SL) is a very popular 3D surface measurement technique where the information about the physical quantity to be measured is stored in the phase of a fringe pattern [10]. Typical arrangements of SL systems consist on stereo-vision configurations which are based on a light source and one or more cameras. Structured light patterns, characterized by a specific structure, are sequentially projected by the light source onto the scene and imaged by the camera(s). The use of SL solves the correspondence problem since artificial features are projected by the projection system on the surface to be reconstructed. The triangulation of corresponding features between projector and camera or between the two cameras, is then used to retrieve 3D information. A calibration process of the optical devices, in terms of lens parameters (focal length, distortion) and geometric parameters, must be carried out in order to obtain accurate surface measurements. The calibration of a stereo-vision system is a two-step process: firstly, the calibration of the individual optical elements must be carried out, then the two individual calibrations are combined to retrieve the relative pose between the stereo pair devices. One of the most commonly adopted camera calibration methodology uses multiple images of a planar checkerboard pattern (with corner points having accurate known positions in the scene) captured by the camera [11]. The checkerboard corners (3D calibration points in the so-called world coordinate system) are used to find a set of word-image correspondences. Typically, from 15 to 20 images, for each camera, are necessary to ensure both an appropriate sampling of the overall working volume and an uniform distribution of the re-projections of the 3D calibration points all over the camera image plane [12, 13]. The overall calibration process thus results time-consuming, since the user need to move either the camera or the planar target in the required different placements and to process the calibration data. Even if there are proposal for semi-automatic camera calibration procedures [13], different optical setups require the use of calibration boards, which can differ for size and number of target points.

This paper proposes an innovative approach for calibrating optical devices, based on the use of an active display to draw the calibration checkerboard. This is achieved by exploiting a conventional computer screen, which allows to display differently sized checkerboard depending on the working volume of the system to be calibrated. The possible non-planarity of the commercial screens is considered and compensated by an iterative approach, which also estimate the actual screen shape during the calibration process. In order to optimize the use of the proposed approach, a study of optimal conditions to calibrate a stereo-camera pair by using a planar checkerboard pattern as calibration target has been carried on. Optimal conditions are defined in terms of the number and the orientation of placements of the calibration board with respect to the stereo-camera pair.

The use of an active display greatly enhances the flexibility of the stereo-camera calibration process since the same device can be used to calibrate different optical setups by simply varying number and size of the displayed squared patterns. Experimental results are finally provided to demonstrate the feasibility of the proposed stereo-camera calibration approach in the 3D measurements of primitive geometries.

1. Background

The correspondences between 3D world physical points and their 2D image camera projections are created by exploiting calibration methods. Many different camera calibration methods have been proposed in technical literature in the last decades [11, 14-18]. One of the most adopted approaches is certainly the Zhang's method [11], also due to a free available dedicated MATLAB® toolbox [13]. This method uses the pin-hole camera model and is based on the homographies between the camera image plane and a planar checkerboard pattern, which is viewed from different placements and orientations. The method is characterized by a high flexibility since either the camera or the planar pattern can be freely and manually moved within the working volume during the calibration process.

Intrinsic and extrinsic camera parameters are firstly estimated with an analytical solution, which is then refined by a non-linear optimization process, which considers both radial and tangential lens distortion up to fourth order. Usually, the objective is to minimize a function based on the error between the 2D real image coordinates and coordinates obtained by re-projecting 3D points according to calibration results.

This approach can be also adopted to calibrate a stereoscopic system. Given two cameras modelled by the pin-hole model, and assuming n images of the calibration template (i = 1, 2, …, n) and s calibration points (j = 1, 2, …, s) for each image, the optimization function F can be expressed as:

$$F = \sum_{i=1}^{n}\sum_{j=1}^{s}\left(\left\|m_{\mathrm{l}}^{ij} - \tilde{m}_{\mathrm{l}}^{ij}\left(k_{1\mathrm{l}}, k_{2\mathrm{l}}, k_{3\mathrm{l}}, k_{4\mathrm{l}}, K_{\mathrm{l}}, R_{\mathrm{l}}^{i}, T_{\mathrm{l}}^{i}, P_{\mathrm{w}}^{j}\right)\right\|^2 + \right.$$
$$\left. + \left\|m_{\mathrm{r}}^{ij} - \tilde{m}_{\mathrm{r}}^{ij}\left(k_{1\mathrm{r}}, k_{2\mathrm{r}}, k_{3\mathrm{r}}, k_{4\mathrm{r}}, K_{\mathrm{r}}, R_{\mathrm{r}}^{i}, T_{\mathrm{r}}^{i}, P_{\mathrm{w}}^{j}\right)\right\|^2\right) \tag{1}$$

where m_l^{ij} and m_r^{ij} represent the real image coordinates of the j-th point in the i-th image on the left and right images, respectively, while $\tilde{m}_{\mathrm{l}}^{ij}\left(k_{1\mathrm{l}}, k_{2\mathrm{l}}, k_{3\mathrm{l}}, k_{4\mathrm{l}}, K_{\mathrm{l}}, R_{\mathrm{l}}^{i}, T_{\mathrm{l}}^{i}, P_{\mathrm{w}}^{j}\right)$ and $\tilde{m}_{\mathrm{r}}^{ij}\left(k_{1\mathrm{r}}, k_{2\mathrm{r}}, k_{3\mathrm{r}}, k_{4\mathrm{r}}, K_{\mathrm{r}}, R_{\mathrm{r}}^{i}, T_{\mathrm{r}}^{i}, P_{\mathrm{w}}^{j}\right)$ represent the reprojected image coordinates of the 3D world point P_{w}, obtained by considering the intrinsic and extrinsic calibration parameters. In particular, k_1 and k_2 are the radial distortion coefficients, k_3 and k_4 are the tangential distortion coefficients, K_{l} and K_{r} are the camera intrinsic matrixes, which contain the focal lengths, (f_{xl}, f_{yl}) and (f_{xr}, f_{yr}) and the principal points ($u_{0\mathrm{l}}$, $v_{0\mathrm{l}}$) and ($u_{0\mathrm{r}}$, $v_{0\mathrm{r}}$), and are expressed as:

$$K_{\mathrm{l}} = \begin{bmatrix} f_{\mathrm{xl}} & 0 & u_{0\mathrm{l}} \\ 0 & f_{\mathrm{yl}} & v_{0\mathrm{l}} \\ 0 & 0 & 1 \end{bmatrix}, \qquad K_{\mathrm{r}} = \begin{bmatrix} f_{\mathrm{xr}} & 0 & u_{0\mathrm{r}} \\ 0 & f_{\mathrm{yr}} & v_{0\mathrm{r}} \\ 0 & 0 & 1 \end{bmatrix} \tag{2}$$

R_{l}, T_{l} and R_{r}, T_{r} represent the extrinsic parameters, which are the rotation matrix and the translation vector that relate the world coordinate system to the image reference frame of the left and right camera, respectively.

1.1. Sensitivity to number and orientations of the checkerboard placements

The conventional calibration procedure is based on a planar checkerboard pattern, which is imaged by the two cameras in different locations and orientations [12]. However, in technical literature there is a lack of strict information about the placements of the calibration target, as well as the number of images to be acquired, in order to obtain acceptable results. In this work, a mylar sheet with printed black and white squares stacked onto a glass plate was used as physical calibration specimen. A set of 21 images was acquired by varying both placement and orientation of the board within the working volume in order to assess the specification required to achieve a robust calibration of a stereo-camera system. This image set was processed to obtain intrinsic and extrinsic parameters of the system, which determined the reference value of a conventional successful calibration. The quality of the obtained calibration parameters was assessed by scanning nominal planar and cylindrical surfaces, thus determining the acquisition accuracy and noise level. The stereo-camera system was indeed coupled with a multimedia DLP projector in order to create a structured light (SL) scanner. A multi-temporal Gray code phase shift profilometry (GCPSP) was used to encode and reconstruct the scene by exploiting a sequence of vertical and horizontal light patterns projected by the video projector [19, 20]. Various image subsets were then selected from the 21 pictures, corresponding to a different number of images. The purpose was to investigate which is the minimum number of images needed for reliable calibration results. In practice, it can be noted that the number of possible subsets is determined by the combinations of the 21 pictures, following the relation:

$$\binom{n}{k} = \frac{n!}{k!(n-k)!} \tag{3}$$

where $n = 21$ is the number of images of the full set, k is the number of images of the studied subset and the [!] operator represents the factorial of the integer. Thus, when $k = 1$, 21 possible combinations are obviously available for different calibrations. When $k = 2$ instead, 210 possible combinations can be determined, while choosing $k = 3$ a total of 1330 combinations can be defined, and so on. A calibration routine was then set up by selecting all the possible image subsets for a given value of k, and by comparing the calibration results with the reference calibration obtained by processing the whole set of 21 images. In this work, $k = 1$, 2 and 3 were considered, since results demonstrated that satisfying calibration results could be obtained. The first assessment between different calibration results was carried out by simply comparing the calibration parameters with respect to the reference values obtained with the 21 different checkerboard placements. A further evaluation was then performed by analyzing the reconstructions of the planar and cylindrical surfaces obtained by exploiting different calibration results, in order to have a clear information about the actual differences in the 3D reconstruction. In particular, the mean distance between corresponding points and the standard deviations σ of those distances were considered. Figure 1 reports the results of the aforementioned comparison: Fig. 1(a), (b) and (c) are referred to subsets composed of one, two and three images, respectively. The horizontal axis reports the index of the combination, while the vertical axis reports the standard deviation of the corresponding set. It is worth noting that the indexes of all the possible combinations are obtained randomly, thus the calibration outcomes are not ordered with any criterion in Fig. 1(a), (b) and (c).

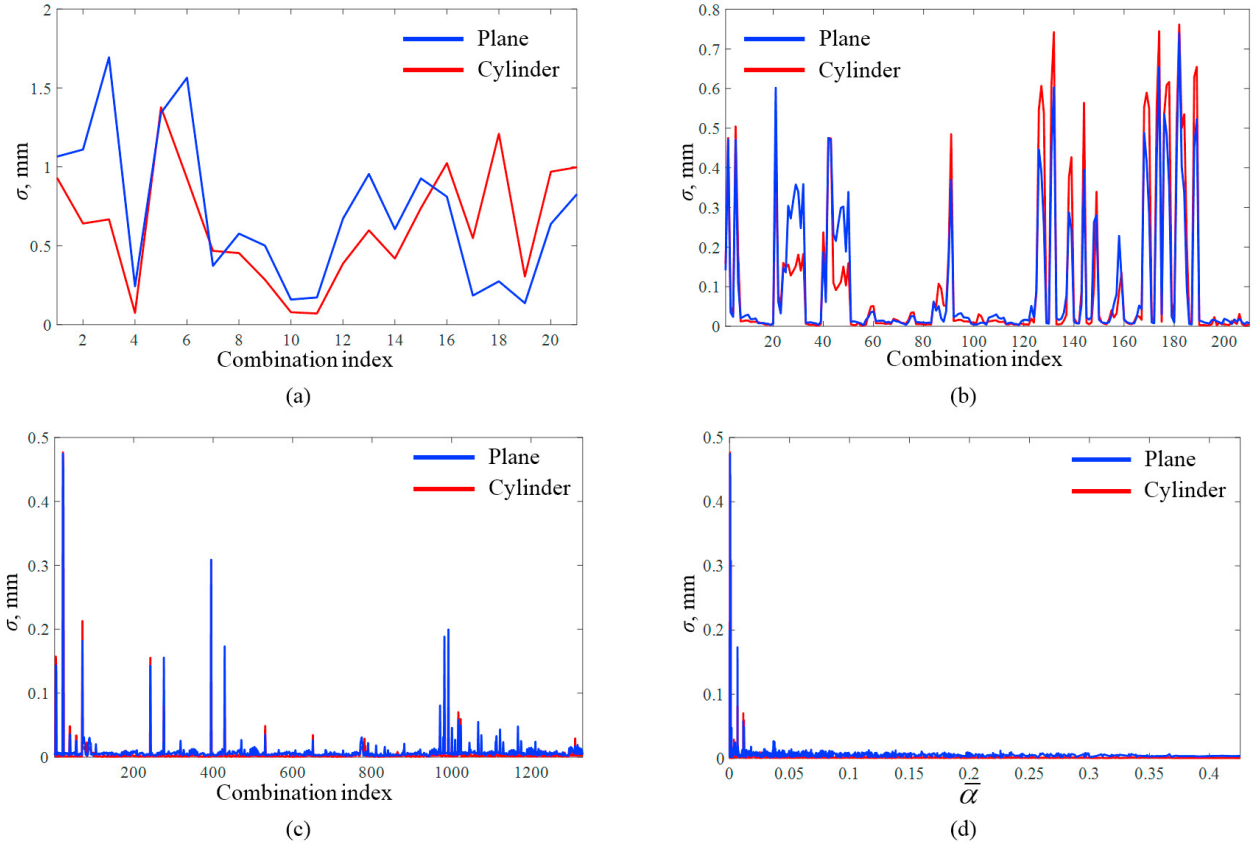

Fig. 1. Reconstruction outcomes in terms of standard deviation of the distances between corresponding points of scans acquired with calibration parameters obtained with a subset of checkerboard placements with respect to the reference calibration: (a) single placement; (b) two placements; (c) three placements; (d) three placements, considering orientations.

Figure 1(a) demonstrates that, obviously, a single image cannot be used to obtain a reliable calibration. Indeed, most of the calibration results led to high standard deviations, in the range of millimeters, meaning that the overall shape of the measured object was erroneously detected. Figure 1(b) instead shows a more reliable trend, since about 75% of the combinations led to a standard deviation which is lower than 0.1 mm. Even if this is not a good result

from the metrological point of view, it can be of interest for applications requiring lower accuracies. On the other hand, Figure 1(c) evidences much more interesting results, since more than 99% of the combinations led to a standard deviation lower than 0.1 mm, and about 90 % led to a standard deviation lower than 5 μm. This result proves that three images can be enough to achieve a robust calibration, also for metrological purposes. Nevertheless, some combinations were found to provide not reliable results, which means that, when only three placements are considered, the checkerboard orientation can't be random. A qualitative analysis shown that the worst calibration results were obtained when two or three checkerboards were almost parallel to each other. This suggested that better results can be achieved when the angles between the checkerboards are relevant, determining an ideal configuration when the checkerboards are mutually perpendicular. Since in practice it may be not feasible to acquire perfectly perpendicular checkerboards, a parameter was defined to assess the quality of the placements corresponding to the 1330 combinations shown in Fig. 1 (c). The normal vectors to each of the calibration planes were computed, namely n_1, n_2 and n_3. Then, a scalar parameter was defined as:

$$\alpha = |(n_i \times n_j) \cdot n_k| \tag{4}$$

where the [×] operator denotes the cross product and the [·] operator denotes the scalar product. By turning the indexes i, j and k, it is possible to obtain three different values of the scalar α, and, finally, to compute the average of these three values (i.e., $\bar{\alpha}$). It is worth noting that the scalar α quantifies how much the n_k normal is parallel to a vector which is perpendicular to both n_i and n_j. Indeed, higher values of α denote that n_k is closer to the perpendicular to both n_i and n_j. Also, higher values of α are obtained when the angle between n_i and n_j is close to $\pi/2$. Thus, the maximum value $\bar{\alpha} = 1$ is obtained when the three normal vectors are perfectly perpendicular in relation to each other. On the other hand, the minimum value $\bar{\alpha} = 0$ is obtained when two normal vectors are perfectly parallel. Figure 1(c) can then be replotted by using the parameter $\bar{\alpha}$ as the horizontal axis, thus obtaining the plot in Fig. 1(d).

Figure 1(d) shows that, indeed, all the combinations characterized by high standard deviations (i.e. low reliability) are in correspondence of low values of the parameters $\bar{\alpha}$. Also, the same figure evidences how the range of reliable values for this scalar is wide, since good calibration results were achieved with $\bar{\alpha} > 0.1$. Finally, the calibration parameters corresponding to the worst and the best calibration obtained using a subset of three images were compared with the reference calibration parameters, as reported in Table 1. This comparison demonstrates that a subset of 3 images can be used to determine calibration parameters, since the obtained values were close to those of the reference calibration.

Table 1. Calibration parameters comparison.

Parameter	Ref. value	Best cal.	Δ	Worst cal.	Δ
f_{xl}, pxl	3628.7	3629.0	0.3792	3462.5	-166.1950
f_{yl}, pxl	3628.6	3629.0	0.3801	3427.8	-200.8444
u_{0l}, pxl	829.7	829.1	-0.6324	640.0	-189.7468
v_{0l}, pxl	609.3	608.8	-0.4801	588.7	-20.6473
f_{xr}, pxl	3660.6	3661.1	0.5589	3412.1	-248.4787
f_{yr}, pxl	3661.5	3662.1	0.6182	3418.3	-243.1881
u_{0r}, pxl	770.2	769.3	-0.8547	776.7	6.4934
v_{0r}, pxl	620.0	619.4	-0.5847	590.3	-29.7257
	0.012	0.012	-0.9e-05	0.011	-0.18 e-02
Ω, rad	0.458	0.458	8.6 e-05	0.430	-2.76 e-02
	-6 e-04	-7 e-04	-7.6 e-05	-3.8 e-03	-0.31 e-02
	-531.6	-531.7	-0.05	-532.6	-0.95
T, mm	3.4	3.4	0.04	4.4	1.00
	122.7	122.9	0.20	114.7	-8.00

2. Proposed calibration approach based on active display

The previous section described the conventional calibration procedure and exposed some systematic and quantitative guidelines to achieve an accurate stereo-camera system calibration. However, the described procedure is based on a conventional calibration specimen, i.e. perfectly planar checkerboard of known sizes, that is difficult to create and very expensive to buy. This could represent a severe limitation in system architecture, since a different physical specimen is needed each time the working volume must vary to fulfill specific needs. Indeed, the same optical setup can be arranged to acquire a variety of fields, thus different specimens, having different sizes, would be needed to calibrate each configuration of the system. This paper proposes a workaround to this issue, by adopting an active display as calibration board. The use of a common LCD screen can give flexibility to the calibration procedure, since different checkerboards can be defined having the required dimensions (i.e. squares size and number) and displayed onto the screen for calibration (Fig. 2). Also, PC screens are always equipped with orientable supports, which makes a lot easier to place the specimen in the needed orientations, as described in the previous section. Thus, the same stereo-camera system used in the previous section was calibrated by using three different placements ($\bar{\alpha} = 0.32$) of a HP ZR2740w screen (2560 × 1440, pixel size 0.2331 mm), and the obtained reprojection error is reported in Fig. 3(a). The figure clearly shows that the reprojection error is high, compared with conventional calibrations. Also, the error distribution is significantly non-Gaussian, thus indicating a poor calibration process. The reliability of the calibration was also assessed by scanning a planar physical checkerboard and comparing the acquired point cloud with the reference best-fit plane. The distances of each measured point with respect to the reference plane are reported in Fig. 4(a). Again, the distances in the figure are significant if compared with the accuracy of conventional stereo systems, which usually is in the order of 0.05 mm. Also, the distances distribution denotes an error in the shape measurement, meaning that the acquired point cloud significantly deviates from the best-fit pane (the distance standard deviation was found to be 0.120 mm). This effect may be ascribed to the non-perfect planarity of the adopted LCD screen. This hypothesis was verified by measuring the same checkerboard used for the calibration with the reference calibration parameter set, showing a double curvature of the screen in the order of 0.1 mm. Then, this measured geometry was used during the system calibration, instead of the theoretical planar grid as conventionally done during calibrations. This allowed to eliminate the distortion effect, and to achieve good calibration results, as demonstrated by Fig. 3 (b) and Fig. 4 (b) (standard deviation 0.061 mm). However, this procedure makes use of an external calibrated system, which is not always available. Therefore, another correction strategy was implemented by adopting an iterative calibration procedure. The first step is driven by considering the screen as perfectly planar. Then, the calibration checkerboard corners are triangulated with the obtained calibration parameters, obtaining curved surfaces instead of planar ones, because of the screen curvature. The measured checkerboard is closer to the actual screen shape then the theoretical planar grid, thus it is used in a further calibration step as the reference geometry. After each calibration step, the reference geometry is updated exploiting the new calibration parameters, and the parameters optimization is started over. Each step of this procedure determines a reduction of the overall reprojection error, in particular by means of its standard deviation. When the reduction of the standard deviation between two consecutive steps is lower than 1%, the procedure is stopped. It is worth noting that this method requires to update the term P_w^j in eq. (1) (i.e., the screen shape), thus even if it can be still accomplished by using 3 screen placements, better results were generally found by adding a further placement of the calibration device. Results obtained with four calibration checkerboard placements are reported in Fig. 4(c) (standard deviation 0.062 mm), showing results which are comparable to the case of Fig. 4(b). The proposed procedure was also tested on two other screens, having different sizes and producers. In all the cases, the simulation outcomes were similar to those shown in Fig. 4(c), proving the effectiveness of the method.

3. Experimental validation

The proposed calibration procedure was validated by exploiting the same active display to calibrate two different stereo-optical setups. The first stereo-rig (i.e., the one used in the previous section) was characterized by two digital cameras with a resolution of 1600 × 1200 pixel (The ImagingSource® DMK 51BU02), equipped with lenses having a 16 mm focal length, and a 1024 × 768 multimedia DLP projector (OPTOMA EX330e, resolution XGA 1024 ×

768 pixel). The optical arrangement was defined to acquire a working volume of about 300 × 300 × 300 mm^3, placed at 1200 mm from the optical devices.

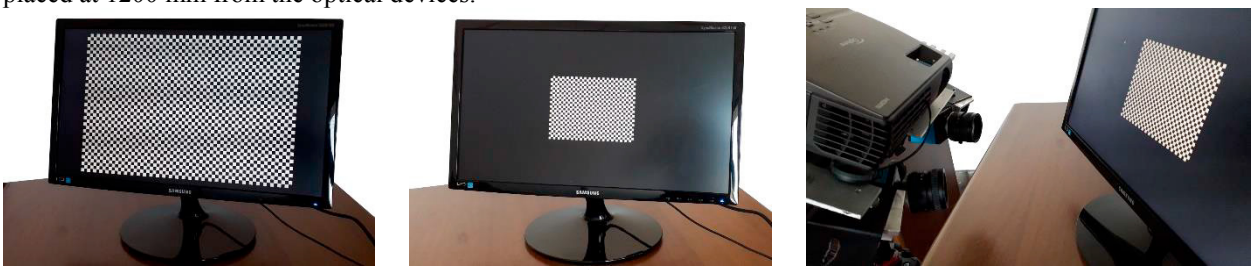

(a) (b) (c)

Fig. 2. Active display: (a) large checkerboard; (b) small checkerboard; (c) stereo-system calibration.

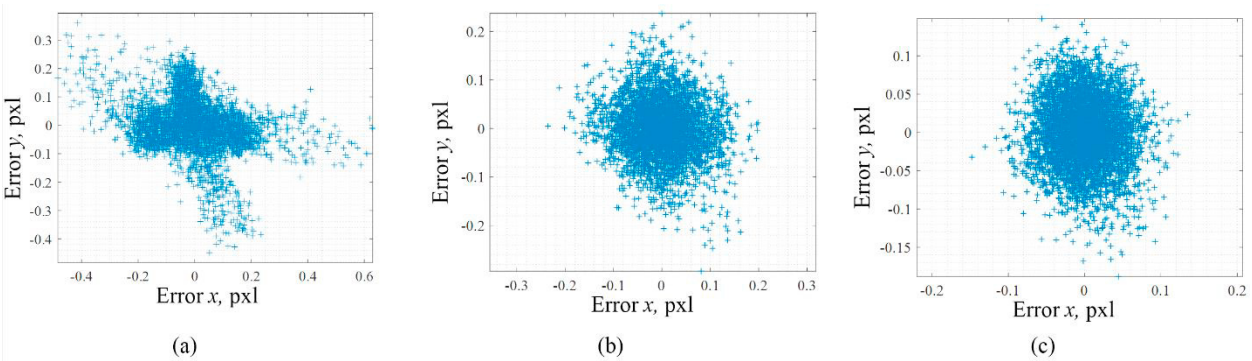

Fig. 3. Reprojection error: (a) neglecting screen curvature; (b) measuring the actual screen curvature; (c) compensating screen curvature.

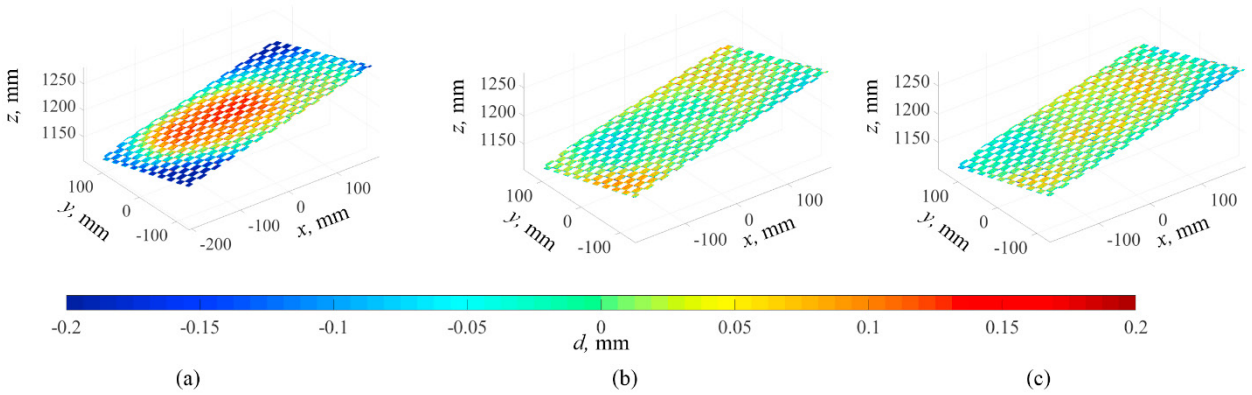

Fig. 4. Plane scanning: (a) neglecting screen curvature; (b) measuring the actual screen curvature; (c) compensating screen curvature.

The calibration results were assessed by scanning a cylinder having a 247.5 mm diameter. Two different point clouds were obtained, one using the calibration parameters obtained with the conventional procedure (i.e., 21 acquisitions of the physical calibration board) and the other using the proposed calibration procedure (i.e., 4 acquisitions of the active display). The point-by-point distance between these two point clouds was then computed, as shown in Fig. 5(a). The maximum distance was found at the cylinder edges, having a value of about 0.06 mm, which is comparable with the system noise level (the overall distance standard deviation was 0.011 mm). Also, the point cloud obtained with the proposed calibration procedure was compared with its best-fit cylinder. This

comparison in reported in Fig. 5(b), showing a low noise level (standard deviation 0.033 mm) and an accurate shape reconstruction since the measured diameter was 247.51 mm.

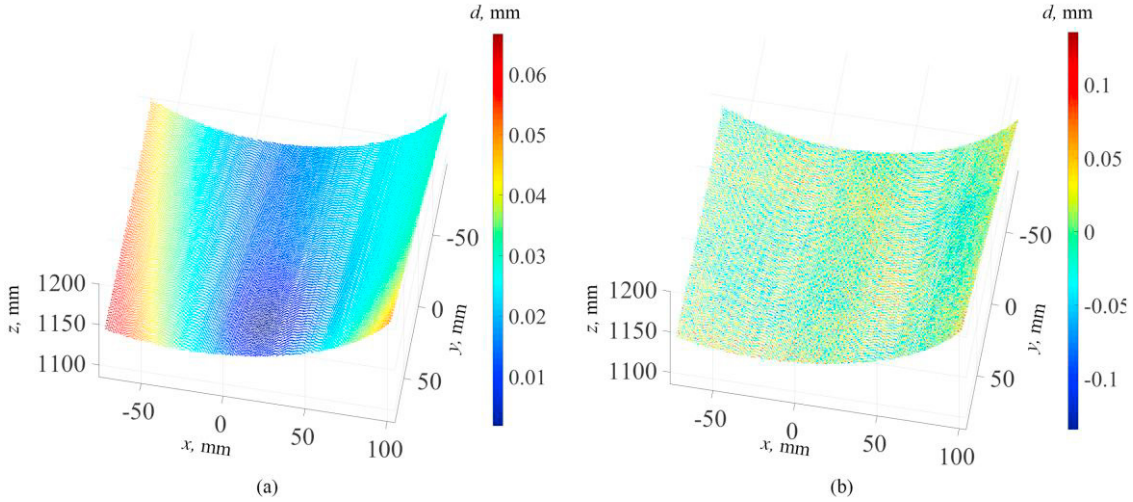

Fig. 5. Cylinder scanning: (a) discrepancies between reconstructions obtained with conventional and proposed procedure; (b) discrepancies with respect to the best-fit cylinder.

Then, another independent system was set up, by assembling the same DLP projector with two digital cameras having resolution of 1280 × 960 pixel (The ImagingSource® DMK 41BU02), equipped with lenses having a 25 mm focal length. This system was calibrated to acquire a smaller working volume of about 60 × 60 × 60 mm^3, placed at 350 mm from the optical devices. It is worth noting that this second system is substantially different from the previous one, both in terms of optical devices and working volume. However, the same active display was successfully used to calibrate the system, only varying the displayed checkerboard sizes to properly fit the camera sensors (Fig. 2 (b)). Again, the system performances were assessed by scanning a planar surface and a cylindrical surface, and by comparing the results with the corresponding best-fit plane and cylinder. Figure 6(a) shows the results obtained for the planar surface, while Figure 6(b) shows the results obtained for the cylindrical surface: in both cases, the noise level is low, and the shape detection is successful (standard deviation of 0.014 mm for the plane and 0.012 mm for the cylinder). Also, the cylinder diameter was measured both with a micrometer and with the stereo system, obtaining 60.10 mm and 60.12 mm values, respectively.

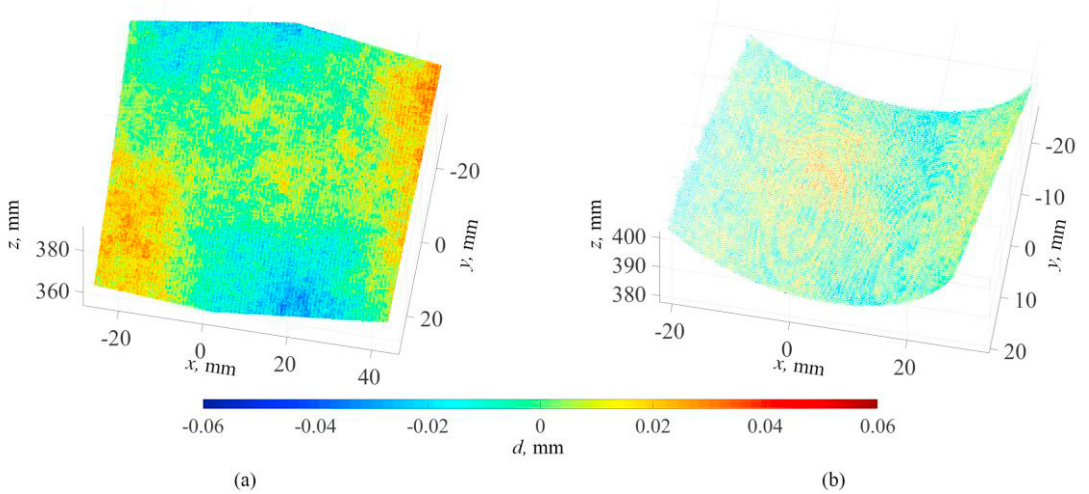

Fig. 6. Discrepancies between reconstructions obtained with the small stereo-system setup with respect to the best-fitting surfaces: (a) plane and (b) cylinder.

4. Conclusions

The present paper presents an innovative approach to carry out the calibration of a stereo camera system. An active display, i.e. a common PC screen, was adopted instead of a physical checkerboard at this purpose, thus gaining flexibility in the definition of the calibration target sizes and number of corners. Firstly, a sensitivity analysis regarding number of placements and orientations of the calibration board for the standard calibration approach was carried out. Results demonstrated that three acquisitions can be adequate to obtain reliable calibration parameters, provided that the acquired checkerboards are placed with relevant angles with respect to each other. Also, a parameter was defined, to numerically determine whether the angles between the checkerboard placements is adequate. The screen-based procedure was then validated, and the non-planarity of the used screen was considered and compensated through an iterative calibration procedure. The results of the proposed approach were evaluated by calibrating two different stereo-vision setups, based on different cameras and working volumes, by displaying differently sized checkerboards on the same screen. The 3D reconstruction of planar and cylindrical surfaces evidenced accurate results in terms of dimensional accuracy and noise level

Acknowledgements

The authors are grateful to the University of Pisa for supporting this research activity (Grant PRA_2018_80).

References

[1] E. Bagci, Reverse engineering applications for recovery of broken or worn parts and re-manufacturing: Three case studies, Adv Eng Softw, 40 (2009) 407-418.
[2] A. Geiger, J. Ziegler, C. Stiller, StereoScan: Dense 3d Reconstruction in Real-time, Ieee Int Veh Sym, (2011) 963-968.
[3] M. Humenberger, C. Zinner, M. Weber, W. Kubinger, M. Vincze, A fast stereo matching algorithm suitable for embedded real-time systems, Comput Vis Image Und, 114 (2010) 1180-1202.
[4] L. Gomes, O.R.P. Bellon, L. Silva, 3D reconstruction methods for digital preservation of cultural heritage: A survey, Pattern Recogn Lett, 50 (2014) 3-14.
[5] F. Bruno, S. Bruno, G. De Sensi, M.L. Luchi, S. Mancuso, M. Muzzupappa, From 3D reconstruction to virtual reality: A complete methodology for digital archaeological exhibition, J Cult Herit, 11 (2010) 42-49.
[6] G.M. Krolczyk, J.B. Krolczyk, R.W. Maruda, S. Legutko, M. Tomaszewski, Metrological changes in surface morphology of high-strength steels in manufacturing processes, Measurement, 88 (2016) 176-185.
[7] P.B. Tang, D. Huber, B. Akinci, R. Lipman, A. Lytle, Automatic reconstruction of as-built building information models from laser-scanned point clouds: A review of related techniques, Automat Constr, 19 (2010) 829-843.
[8] M. Javaid, A. Haleem, Additive manufacturing applications in orthopaedics: A review, Journal of Clinical Orthopaedics and Trauma, 9 (2018) 202-206.
[9] S. Van der Jeught, J.J.J. Dirckx, Real-time structured light profilometry: a review, Optics and Lasers in Engineering, 87 (2016) 18-31.
[10] C. Zuo, S.J. Feng, L. Huang, T.Y. Tao, W. Yin, Q. Chen, Phase shifting algorithms for fringe projection profilometry: A review, Optics and Lasers in Engineering, 109 (2018) 23-59.
[11] Z.Y. Zhang, A flexible new technique for camera calibration, Ieee T Pattern Anal, 22 (2000) 1330-1334.
[12] Z. Zhang, Flexible Camera Calibration by Viewing a Plane from Unknown Orientations, International Conference on Computer Vision, 1999, pp. 666-673.
[13] J.Y. Bouguet, Camera calibration toolbox for Matlab. available: http://www.vision.caltech.edu/bouguetj/calib_doc/. 2015 (accessed 11 May 2018).
[14] R.Y. Tsai, A Versatile Camera Calibration Technique for High-Accuracy 3d Machine Vision Metrology Using Off-the-Shelf Tv Cameras and Lenses, Ieee T Robotic Autom, 3 (1987) 323-344.
[15] J. Heikkila, O. Silven, A four-step camera calibration procedure with implicit image correction, 1997 Ieee Computer Society Conference on Computer Vision and Pattern Recognition, Proceedings, (1997) 1106-1112.
[16] Q. Chen, H.Y. Wu, T. Wada, Camera calibration with two arbitrary coplanar circles, Computer Vision - Eccv 2004, Pt 3, 3023 (2004) 521-532.
[17] M. Agrawal, L.S. Davis, Camera calibration using spheres: A semi-definite programming approach, Ninth Ieee International Conference on Computer Vision, Vols I and Ii, Proceedings, (2003) 782-789.
[18] R. Orghidan, J. Salvi, M. Gordan, B. Orza, Camera calibration using two or three vanishing points, Fed Conf Comput Sci, (2012) 123-130.
[19] S. Barone, P. Neri, A. Paoli, A.V. Razionale, Structured light stereo catadioptric scanner based on a spherical mirror, Optics and Lasers in Engineering, 107 (2018) 1-12.
[20] S. Barone, P. Neri, A. Paoli, A.V. Razionale, Catadioptric stereo-vision system using a spherical mirror, Procedia Struct Inte, 8 (2018) 83-91.